

Quantum Many-Body Scars for Arbitrary Integer Spin in $2 + 1$ D Abelian Gauge Theories

Thea Budde, Marina Krstic Marinkovic, and Joao C. Pinto Barros

Institut für Theoretische Physik, ETH Zürich, Wolfgang-Pauli-Str. 27, 8093 Zürich, Switzerland

(Dated: March 29, 2024)

The existence of Quantum Many-Body Scars has been established across different quantum many-body systems, including spin-1/2 Quantum Link Models. We systematically identify scars for pure gauge theories with arbitrarily large integer spin S in $2 + 1$ D, concretely for Truncated Link Models, where the electric field is truncated rather than replaced by spins. Through an explicit analytic construction, we show that the presence of scars is widespread. We confirm these findings numerically for small truncated spin and $S = 1$ Quantum Link Models. The proposed analytic construction establishes the presence of scars far beyond volumes and spins that can be probed with existing numerical methods.

Introduction.— Starting with an initial state and the microscopic Hamiltonian of an isolated system governing its dynamics, it might seem that the unitary evolution of the system would prevent thermalization. This puzzle is addressed by the Eigenstate Thermalization Hypothesis (ETH) [1–5]. According to the ETH, for non-integrable systems, the high-energy states and the observables of interest will eventually converge to a description in accordance with equilibrium statistical mechanics, achieving thermal equilibrium. In contrast to the ETH, many-body localized systems defy this trend due to their emergent integrability [6]. Systems exhibiting Quantum Many-Body Scars (QMBS) offer a contrasting example [7–9]. They also evade ETH, but only in an exponentially small fraction of states in the Hilbert space.

The effect of QMBS was first observed in a Rydberg-atom quantum simulator, marked by persistent revivals for particular initial states, in contrast to the vast majority of other high-energy initial states [10, 11]. In parallel with the exact construction of highly excited eigenstates in a non-integrable model [12, 13], the experiment has sparked intense research across different systems, where a *weak* breaking of the ETH takes place [14–26]. In this case, the presence of *few* anomalous eigenstates, can leave an imprint on thermalization. Among their special features is that they are characterized by atypically low entanglement entropy, compared with other states arbitrarily close in the spectrum. This is in stark contrast to what is expected from the ETH. In particular, QMBS may exhibit an area law. This means that the entanglement between a subsystem and its complement is proportional to the area of the boundary that divides them. In turn, highly excited states are expected to have an entanglement that grows linearly with the volume of the subsystem.

The interplay between gauge symmetry and scarring phenomena is not fully understood. Gauge theories naturally lead to constraints, and specific constraints can give rise to QMBS, as observed in the PXP model [10, 27, 28]. Gauge theories also feature local symmetries, which segment the Hamiltonian into distinct sectors that do not

mix under time evolution. Supplied by a condition on physical states, this leads to local constraints in the form of Gauss’ law. Beyond the PXP model, QMBS have also been observed in other gauge theories, such as the Abelian case in the presence of matter in $1 + 1$ D [29], pure gauge in $2 + 1$ D [30–32] and non-Abelian in $2 + 1$ D [33]. So far, the research on QMBS in Abelian pure gauge theories has exclusively focused on spin-1/2 Quantum Link Models (QLM) [30–32], which also exhibit other interesting phenomena such as crystalline confining phases or confining strings with fractionalized electric flux strands [34–37]. This Letter demonstrates, for the first time, the existence of QMBS in link models with arbitrary integer spins.

Addressing questions related to real-time dynamics falls outside the capabilities of conventional lattice gauge theory methods, as Monte Carlo simulations face inefficiencies due to severe sign problems associated with real-time processes (see e.g. [38, 39]). Sign problems have motivated the development of the field of quantum simulations of gauge theories [40–45]. Formulations like QLMs are essential for preserving gauge symmetry while ensuring a finite Hilbert space for a finite lattice volume. Recovering the theory in the continuum limit may take different routes [46–52]. No matter the path, the road ahead is long until we can make decisive contributions to theories like Quantum Chromodynamics (QCD). Hence, it is imperative to pinpoint intriguing phenomena that can drive experiments along this path. The study of QMBS is a meritorious example as it is present in simple gauge theories and probes fundamental aspects of quantum many-body theory.

Demonstrating the presence of QMBS for large Hilbert spaces per gauge link, beyond spin-1/2, serves several fundamental purposes: it directly addresses how widespread QMBS are across many-body systems; it reveals novel mechanisms for their formation, illuminating the role played by gauge symmetry; and it helps to guide quantum simulation experiments toward interesting questions before the necessary complexity of QCD is achieved.

In this Letter, we demonstrate the extensive presence of QMBS across $2 + 1$ dimensional $U(1)$ gauge theories without matter. Concretely, we explicitly construct mid-spectrum states that satisfy area law entanglement for arbitrary integer spin, specifically for a simply truncated Hilbert space per link. We further verify the existence of these states by numerically determining the system's eigenstates and calculating their entanglement and Shannon entropy for spin 1 and 2. Our findings unveil the presence of QMBS for single-leg ladders of the spin-1 QLM, which are more accessible to experiments than larger systems. Furthermore, our analytical approach allows us to identify QMBS for arbitrary integer spin and system size, circumventing the limitations of existing numerical methods when applied to large dimensional Hilbert spaces.

Link models in $2+1D$.— We consider models on square $L_1 \times L_2$ lattices with bosonic degrees of freedom living on the links

$$H = \sum_n \left(U_{n1}^\dagger U_{n+1\hat{2}}^\dagger U_{n2} U_{n+\hat{2}1} + \text{h.c.} \right) + V, \quad (1)$$

where the indices $n \equiv (n_1, n_2)$ represent lattice sites, while the labels $i \in \{1, 2\}$ represent the two directions. The first terms of the Hamiltonian are plaquette terms constructed by acting on each of the four links of a plaquette with operators represented by U . The term V , which we will call generically *potential*, will always be diagonal in the electric field E_{ni} . The commutation relations between these variables are $[E_{mi}, U_{nj}] = U_{mi} \delta_{mn} \delta_{ij}$. Under these general conditions, the Hamiltonian has a set of local symmetries. Concretely, there is one generator of local gauge transformations G_n per lattice site, which commutes with the Hamiltonian

$$G_n = E_{n1} + E_{n2} - E_{n-\hat{1}1} - E_{n-\hat{2}2}, \quad [H, G_n] = 0. \quad (2)$$

We will use the electric field basis, denoted by $|\varepsilon\rangle$ for a single link. The generators G_n are diagonal in this basis. The Hilbert space breaks into many different sectors. We will focus on the physical sector characterized by the Gauss' law $G_n |\psi\rangle = 0$, for all sites, which acts as a constraint of the system.

The model also has two winding symmetries. Concretely, the observables $W_1 = \sum_{n_1=0}^{L_1-1} E_{(n_1, m)2}$ and $W_2 = \sum_{n_2=0}^{L_2-1} E_{(m, n_2)1}$ commute with the Hamiltonian. In the physical sector, their eigenvalues are independent of m . We focus on the zero-winding sector $W_i |\psi\rangle = 0$ for both $i = 1$ and $i = 2$. This is the largest sector of the theory. There are further global symmetries that depend on the choice of the potential and are used to reduce the size of the Hilbert space in exact diagonalization calculations. They are described in the Supplementary Material [53]. We will be interested in two specific versions of this model that ensure that we will have a finite-dimensional Hilbert space per link.

In Quantum Link Models (QLM) [48, 54, 55] U_{ni}/U_{ni}^\dagger are spin raising/lowering operators. U_{ni} and U_{ni}^\dagger do not commute and act according to $U|\varepsilon\rangle \propto \sqrt{S(S+1) - \varepsilon(\varepsilon+1)}|\varepsilon+1\rangle$. The electric field operators E correspond to the z component spin operators.

In Truncated Link Models (TLM) [29] the electric field is simply truncated, meaning $U|S\rangle = 0$, $U^\dagger| -S\rangle = 0$ and $U|n\rangle = |n+1\rangle$ otherwise. U_{ni} and U_{ni}^\dagger still do not commute, though the non-zero commutation relation is removed to the edge of the local Hilbert space (to the states $| -S\rangle$ and $|S\rangle$). With this construction, there will be $2S+1$ states per link. We generically refer to S as the total spin, irrespective of the formulation we are using. The $S = 1$ TLM is equivalent to the $S = 1$ QLM.

For the Hamiltonian (1) we will also write

$$H = K + V, \quad K = H^+ + H^-, \quad H^\pm = \sum_n H_n^\pm, \quad (3)$$

where $H_n^- = U_{n1}^\dagger U_{n+1\hat{2}}^\dagger U_{n2} U_{n+\hat{2}1}$ and $H^+ = (H^-)^\dagger$ are *kinetic operators*. This notation follows the convention that we will adopt throughout the letter. ‘‘Plaquette at site n ’’ refers to the plaquette for which n is its lower left vertex. In order to simplify the formulas we will also adopt the convention $(H^+)^{-m} \equiv (H^-)^m$. This should not be confused with the inverse of $(H^+)^m$, since these operators are not invertible.

Zero-mode scars.— We refer to zero-modes as eigenstates of the plaquette term of the Hamiltonian with zero eigenvalues. In our notation, these states satisfy

$$K|\psi_z\rangle = \sum_n (H_n^+ + H_n^-)|\psi_z\rangle = 0. \quad (4)$$

Zero-modes can play a crucial role in forming quantum many-body scars. Systems with a spectral symmetry, together with point-group symmetries, can exhibit an exponential number of zero-modes [56]. Their existence follows from an index theorem, which we review and adapt to our models of interest in the Supplementary Material [53]. While one might expect these eigenstates to be thermal, it has been shown that low entangled states can be constructed within this subspace for specific cases. It was further conjectured that this is a generic property of local Hamiltonians with an exponential number of zero-modes [57]. Such a result was also observed in the case of gauge theories in the spin-1/2 QLM, even if it is possible to find scars that are not constructed exclusively from zero-modes [31, 32].

We show that it is also possible to construct such states for arbitrary spin truncated link models. The number of these low entropy states grows exponentially with volume. By choosing appropriately the potential term of the Hamiltonian, different linear combinations can be isolated as low entropy eigenstates. To establish these states as scars, one should show that the model in question is non-integrable. It is expected that this is the

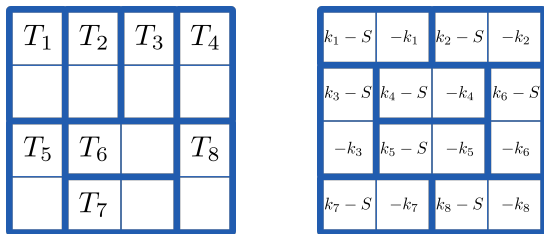


FIG. 1. Left: Example of a tiling T of the 2D lattice, consisting of partitioning it into 2×1 and 1×2 tiles, to a total of 8 tiles. Right: Representation of a scar state based on an alternative tiling and in the dual representation. An independent sum over every k_i with a weight of $\prod_i (-1)^{k_i}$ is assumed. See Eq. (5).

case for pure gauge theories in (2+1)-d, and we further demonstrate this for a single-leg ladder with $S = 1$ in the Supplementary Material [53].

QMBS in TLM with arbitrary integer spin.— Next, we show that zero-modes with area-law entanglement entropy exist in truncated link models of all integer spins. We start by partitioning the 2D lattice into 2×1 and 1×2 tiles, as depicted on the left of Fig. 1. A given partition will be called tiling and will be denoted by T . It can be represented by a set of tuples (n, n') where the two entries indicate the two plaquettes making up each tile. We then define the states

$$|\psi_s^{(i,T)}\rangle = \frac{1}{(S+1)^{|T|/2}} \prod_{(n,n') \in T} \left(\sum_{k=0}^S (-1)^k (H_n^+)^{i-S+k} (H_{n'}^+)^{i-k} \right) |\mathbf{0}\rangle, \quad (5)$$

where $|\mathbf{0}\rangle$ is the state where all links have value zero, and $0 \leq i \leq S$. The states $|\psi_s^{(i,T)}\rangle$ have the property $(H_m^- + H_{m'}^+) |\psi_s^{(i,T)}\rangle = (H_m^+ + H_{m'}^-) |\psi_s^{(i,T)}\rangle = 0$ if (m, m') is a tile in T . Therefore,

$$K |\psi_s^{(i,T)}\rangle = \sum_{(n,n') \in T} (H_n^+ + H_{n'}^- + H_n^- + H_{n'}^+) |\psi_s^{(i,T)}\rangle = 0, \quad (6)$$

making them zero-modes.

These states are zero-modes in all lattices where $L_1 L_2$ is even. The number of possible tilings grows exponentially with $L_1 L_2$ if both L_1 and L_2 are larger than 1.

By partitioning the systems into two regions, we see that the entanglement between them is generated by tiles that touch both regions resulting in an area law. The states $|\psi_s^{(i,T)}\rangle$ are then mid-spectrum states with area law entanglement entropy, making them quantum scars.

To get a deeper understanding of the structure of these scars, and to connect them to lego scars that have been constructed in the $S = 1/2$ QLM, it is useful to define the *dual basis* for integer spin. Height variables $h_n \in \mathbb{Z}$ live at the center of plaquettes. The values of the vertical

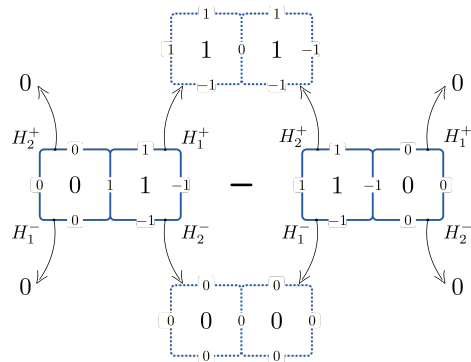


FIG. 2. Schematic depiction of the scar building block for $S = 1$. The tiles depicted with solid lines make up the scar state. The operators H_n^\pm raise or lower the height variables in plaquette n . They either annihilate the state or generate another state, depicted with dashed lines. This is canceled by applying the other type of operator on the second state.

links are given by the difference of the height variables of the plaquettes to their right and left, while the values of the horizontal links are given by the difference of the height variables of the plaquettes to their bottom and top, i.e. $E_{n1} = h_{n-\hat{2}} - h_n$ and $E_{n2} = h_n - h_{n-\hat{1}}$. Height variable configurations with $|h_n - h_{n'}| \leq S$ for all neighboring plaquettes n, n' represent a valid spin- S link configuration.

The height variable representation with periodic boundary conditions is not unique, since adding a constant to all height variables gives the same state. If there is an open boundary condition in at least one direction, we set all height variables at one open boundary to have the value of the neighboring boundary link. In our construction, we always choose the top boundary, which makes the representation unique. The kinetic operators H_n^+ and H_n^- , are raising/lowering operators for the height variable h_n .

In the dual representation, the state (5) in a 2×1 plaquette system is

$$|\psi_i\rangle = \frac{1}{\sqrt{S+1}} \sum_{k=0}^S (-1)^k |(i-S+k) (i-k)\rangle \quad (7)$$

where the state is labeled with its height variables $|h_1 h_2\rangle = (H_1^+)^{h_1} (H_2^+)^{h_2} |\mathbf{0}\rangle$. An illustration of this tile and the terms that cancel each other in the sum $K |\psi_i\rangle$ for $S = 1$ can be found in Fig. 2.

All states that contribute in (5) have a height variable representation where there is one state out of the sum (7) on all tiles of the tiling T . The state sums over all $(S+1)^{|T|}$ combinations of these states. A pictorial representation of this tiling is shown on the right-hand side of Fig. 1. This tiling structure is similar to the lego and sub-lattice scars constructed for the $S = 1/2$ case [31, 32], and allows for the construction of an exponential number of scars for arbitrary truncated link models. A formal

definition of this tiling, in the form of a tiling product, can be found in the Supplementary Material [53]. There, we also describe a more general framework to construct more low-entropy zero-modes in TLMs.

Numerical results and discussion.— While these states are low entropy zero-modes, they are degenerate with all the other zero-modes and are not easily identifiable in the spectrum. In the following, we introduce a potential that has these states as eigenstates. By analyzing the Shannon entropy and the bipartite entanglement entropy of the eigenstates of the Hamiltonian, we verify the existence of these low entropy states numerically. See the Supplementary Material for a brief overview of the calculation of these quantities as used in this work [53].

From Eq. (7) we see that the sum of the height variables remains constant and equal to $(2i - S)$ over the entire sum. This does not mean that the sum over height variables is a valid potential because, in general, the height variables are not uniquely defined from the physical configuration. But they can be made unique for open boundary conditions, as described above. For example, in the case of a single-leg ladder, the sum of all height variables can be seen as the sum of the horizontal links of the top row. In general, for open boundary conditions, we write

$$V = \lambda \sum_n h_n, \quad (8)$$

which will have the constructed scars as eigenstates with energy $E = \lambda \frac{L_1 L_2}{2} (2i - S)$.

For $S = 1$ the two zero-mode tiles are

$$|\psi_{\pm}\rangle = \frac{1}{\sqrt{2}}(|0 \pm 1\rangle - |\pm 1 0\rangle), \quad (9)$$

which correspond to choosing $i = 1$ and $i = 0$ in (7). We first study a $S = 1$ single-leg ladder with L plaquettes. This is a chain of plaquettes with periodic boundary conditions in the direction of the chain, but not the direction perpendicular to it. For such a ladder, there are exactly two distinct tilings of 2×1 tiles. They correspond to placing the lower left corner of the tiles in either even or odd sites. These two states, coming from two different tilings with the same i , are not orthogonal but generate a two-dimensional scarred Hilbert space. We then expect four scars. Two degenerate low entropy states with energy $L\lambda/2$ from the tilings of state $|\psi_{+}\rangle$ ($i = 1$) and two with energy $-L\lambda/2$ from tilings of state $|\psi_{-}\rangle$ ($i = 0$). This is exactly what is observed when performing exact diagonalization on small systems, the results of which are presented in Fig. 3. The four low-entropy states are clearly identifiable and each of them is composed of the expected states.

For systems with a larger vertical direction, there are many more ways to tile the plane with 2×1 and 1×2 tiles. Adding a second leg is enough to make the number of possible tilings exponentially large, all of which will mix

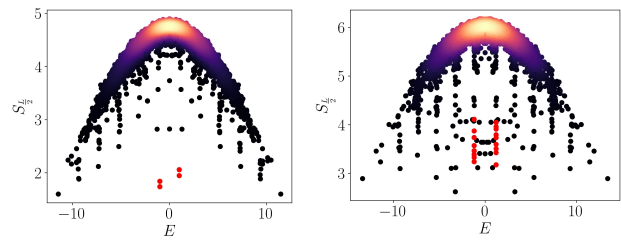


FIG. 3. Left: Entanglement entropy of a $S = 1$ ladder with 10×1 plaquettes using the potential (8) with $\lambda = 0.2$. Four mid-spectrum states with low entropy, shown in red, are visible. They are superpositions of the predicted states. For the remaining states, brighter colors indicate a higher density of states. Right: Entanglement entropy of 6×2 $S = 1$ plaquettes with periodic boundary conditions in the x direction and $\lambda = 0.2$ in the zero momentum sector. Many mid-spectrum states with low entropy are present. The towers marked in red contain the predicted states.

in the spectrum. Using the sum of the height variables as the potential, we expect towers of low-entropy states at energy $\pm L_1 L_2 \lambda / 2$. These two towers are observed, as depicted in Fig. 3. There are many other low-entropy states at other energies, which make use of vertical tiles. They entail a further structure, that allows the number of height variables with value 1 not to be the same as the ones with value 0. While these are still scars built up from zero-modes, we do not expect this construction to be generalizable beyond $2 \times L$ systems and will not attempt a detailed characterization here. For periodic lattices, we studied the 4×4 system with a generalized version of the potential. There the expected scar towers are also present. Details for this case can be found in the Supplementary Material [53].

Instead of the designed potential that was used to isolate the constructed scars, one might want to use the standard electric field term

$$V = g \sum_n E_n^2. \quad (10)$$

This potential exhibits scars that are constructed from zero-modes and allows for the identification of new tiling patterns. We identify three low entropy states in a 4×4 lattice, which turn out to be constructed from zero-modes (see Fig. 4). Two of these are generalizable to arbitrary $L_1 \times L_2$ lattices if both L_i are even. We characterize one of them here, the remaining two scars are described in the Supplementary Material [53].

The scar has the form (5), just as the other scars we derived. However, the two plaquettes that make up tiles do not share a link, but neighbor each other diagonally in a pattern depicted in Fig. 4. This is still a zero-mode since each plaquette has one neighbor with height ± 1 in all configurations and may therefore never take height ∓ 1 itself. The state is an eigenstate of (10) because the number of neighbors with height ± 1 is always the same

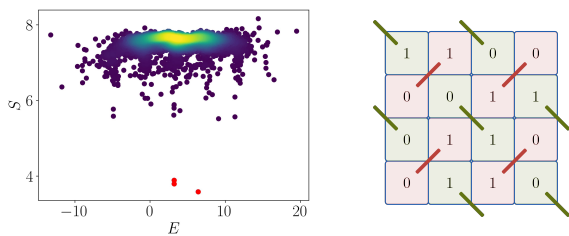


FIG. 4. Left: Shannon entropy of 4×4 $S = 1$ plaquettes with periodic boundary conditions using the E^2 potential (10) with $g = 0.2$ in the zero momentum and $+1$ charge conjugation sectors. Three mid-spectrum states with low entropy, are visible and colored in red. Bright colors indicate a higher density of states. Right: Illustration of a $S = 1$ zero-mode that is an eigenstate of $\sum_n E_n^2$. A sublattice structure is built by singlet states of two plaquettes connected diagonally. Plaquettes connected by red or green lines form tiles.

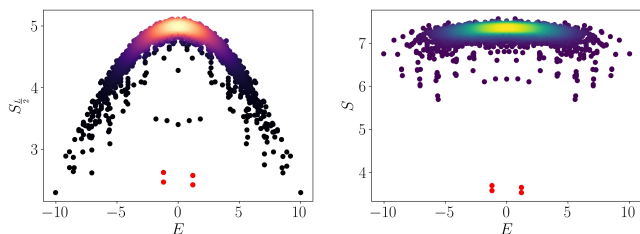


FIG. 5. Left: Entanglement entropy of a $S = 2$ Ladder with 6 plaquettes with $\lambda = 0.2$. Brighter colors indicate a higher density of states. Right: Shannon entropy of a $S = 2$ Ladder with 6 plaquettes with $\lambda = 0.2$. Four mid-spectrum states with low entropy are visible, colored in red. The remaining two predicted states are mixed with a tower of zero-modes at $E = 0$.

for both plaquettes of each tile. This means that in all configurations, half of the links have values ± 1 and the others are 0. Establishing the presence of these scars beyond $S = 1$ is beyond the scope of this work. Systems with larger spins are less accessible through ED beyond single-leg ladders and we did not observe any of these scars for $S \leq 2$ in this case.

For $S = 2$ we have studied the 6×1 ladder in Fig. 5 with the height potential (8). In this case, we expect scars obtained from choosing $i = 0$, $i = 1$, and $i = 2$ in (7). The $i = 1$ scar has zero energy for any value of λ , while the other two will have $E_{2,1} = \pm 6\lambda$. The latter two are evident in the figure. The $i = 1$ scar is not visible, since it is in superposition with a tower of zero-modes.

This demonstrates the existence of low entanglement entropy zero-modes in systems beyond $S = 1$. For larger volume or higher spin systems, we have established theoretically the existence of such states in the earlier sections of this article.

Conclusions and outlook.— In this Letter, we demonstrate that QMBS exist across various 2D Abelian gauge theories. In the limit of zero coupling, a spectral sym-

metry emerges, leading to an exponentially large number of zero-modes. We show that it is possible to construct many states with area-law entanglement entropy, despite these states being in the middle of the spectrum. The number of these states grows exponentially with the volume, but they still comprise an exponentially small fraction of the Hilbert space, indicating weak ETH breaking.

We have analytically constructed QMBS for arbitrary truncated spins, revealing their existence beyond the reach of existing numerical methods, thereby marking a significant step towards understanding their role in the continuum limit, where the Hilbert space per link is not bounded. Our construction relies on the existence of numerous zero-modes, common in QLMs for arbitrary spin, though our method extends only to $S=1$ QLMs. This does not exclude that scars in higher spin QLMs exist but a different constructive approach might be needed. For $S = 1$, some scars survive the presence of the standard $g \sum_n E_n^2$ potential. In a recent work [58], it has been argued that scars originally present on single-leg ladders $SU(2)$ gauge theories disappear once larger truncations of the Hilbert space are considered. Our results for $S = 1$ show that these systems might be too simple to observe scars with the E^2 potential. An interesting generalization of our findings would involve extending the explicit QMBS construction to non-Abelian theories like $SU(2)$. From the experimental side, our theoretical description can guide future detection of QMBS and investigations of weak ergodicity breaking in systems inaccessible through classical simulations.

Acknowledgements.— We are grateful to Debasish Banerjee for insightful discussions. T.B. thanks the Galileo Galilei Institute for Theoretical Physics for the hospitality during the completion of part of this work. This research was supported by the Munich Institute for Astro-, Particle and BioPhysics (MIAPbP), which is funded by the Deutsche Forschungsgemeinschaft (DFG, German Research Foundation) under Germany’s Excellence Strategy – EXC-2094 – 390783311. We acknowledge access to Piz Daint at the Swiss National Supercomputing Centre, Switzerland under the ETHZ’s share with the project ID eth8. Support from the Google Research Scholar Award in Quantum Computing and the Quantum Center at ETH Zurich is gratefully acknowledged.

Note.— During the final stages of our manuscript, we became aware of another work [59] on quantum many-body scarring in a 2+1D $U(1)$ gauge theory with dynamical matter.

[1] J. M. Deutsch, Quantum statistical mechanics in a closed system, Physical review a **43**, 2046 (1991).

- [2] M. Srednicki, Chaos and quantum thermalization, *Physical review e* **50**, 888 (1994).
- [3] M. Rigol, V. Dunjko, and M. Olshanii, Thermalization and its mechanism for generic isolated quantum systems, *Nature* **452**, 854 (2008).
- [4] L. D'Alessio, Y. Kafri, A. Polkovnikov, and M. Rigol, From quantum chaos and eigenstate thermalization to statistical mechanics and thermodynamics, *Advances in Physics* **65**, 239 (2016).
- [5] J. M. Deutsch, Eigenstate thermalization hypothesis, *Reports on Progress in Physics* **81**, 082001 (2018).
- [6] D. A. Abanin, E. Altman, I. Bloch, and M. Serbyn, Colloquium: Many-body localization, thermalization, and entanglement, *Reviews of Modern Physics* **91**, 021001 (2019).
- [7] M. Serbyn, D. A. Abanin, and Z. Papić, Quantum many-body scars and weak breaking of ergodicity, *Nature Physics* **17**, 675 (2021).
- [8] S. Moudgalya, B. A. Bernevig, and N. Regnault, Quantum many-body scars and hilbert space fragmentation: a review of exact results, *Reports on Progress in Physics* **85**, 086501 (2022).
- [9] A. Chandran, T. Iadecola, V. Khemani, and R. Moessner, Quantum many-body scars: A quasiparticle perspective, *Annual Review of Condensed Matter Physics* **14**, 443 (2023).
- [10] H. Bernien, S. Schwartz, A. Keesling, H. Levine, A. Omran, H. Pichler, S. Choi, A. S. Zibrov, M. Endres, M. Greiner, *et al.*, Probing many-body dynamics on a 51-atom quantum simulator, *Nature* **551**, 579 (2017).
- [11] D. Bluvstein, A. Omran, H. Levine, A. Keesling, G. Semeghini, S. Ebadi, T. T. Wang, A. A. Michailidis, N. Maskara, W. W. Ho, S. Choi, M. Serbyn, M. Greiner, V. Vuletić, and M. D. Lukin, Controlling quantum many-body dynamics in driven rydberg atom arrays, *Science* **371**, 1355–1359 (2021).
- [12] S. Moudgalya, S. Rachel, B. A. Bernevig, and N. Regnault, Exact excited states of nonintegrable models, *Physical Review B* **98**, 235155 (2018).
- [13] S. Moudgalya, N. Regnault, and B. A. Bernevig, Entanglement of exact excited states of affleck-kennedy-lieb-tasaki models: Exact results, many-body scars, and violation of the strong eigenstate thermalization hypothesis, *Physical Review B* **98**, 235156 (2018).
- [14] C. J. Turner, A. A. Michailidis, D. A. Abanin, M. Serbyn, and Z. Papić, Weak ergodicity breaking from quantum many-body scars, *Nature Physics* **14**, 745–749 (2018).
- [15] W. W. Ho, S. Choi, H. Pichler, and M. D. Lukin, Periodic orbits, entanglement, and quantum many-body scars in constrained models: Matrix product state approach, *Physical review letters* **122**, 040603 (2019).
- [16] V. Khemani, C. R. Laumann, and A. Chandran, Signatures of integrability in the dynamics of rydberg-blockaded chains, *Physical Review B* **99**, 161101 (2019).
- [17] S. Choi, C. J. Turner, H. Pichler, W. W. Ho, A. A. Michailidis, Z. Papić, M. Serbyn, M. D. Lukin, and D. A. Abanin, Emergent $su(2)$ dynamics and perfect quantum many-body scars, *Physical review letters* **122**, 220603 (2019).
- [18] M. Schechter and T. Iadecola, Weak ergodicity breaking and quantum many-body scars in spin-1 x y magnets, *Physical review letters* **123**, 147201 (2019).
- [19] D. K. Mark and O. I. Motrunich, η -pairing states as true scars in an extended hubbard model, *Physical Review B* **102**, 075132 (2020).
- [20] D. K. Mark, C.-J. Lin, and O. I. Motrunich, Unified structure for exact towers of scar states in the affleck-kennedy-lieb-tasaki and other models, *Physical Review B* **101**, 195131 (2020).
- [21] G.-X. Su, H. Sun, A. Hudomal, J.-Y. Desaulles, Z.-Y. Zhou, B. Yang, J. C. Halimeh, Z.-S. Yuan, Z. Papić, and J.-W. Pan, Observation of many-body scarring in a bose-hubbard quantum simulator, *Physical Review Research* **5**, 023010 (2023).
- [22] J. C. Halimeh, L. Barbiero, P. Hauke, F. Grusdt, and A. Bohrdt, Robust quantum many-body scars in lattice gauge theories (2022), arXiv preprint arXiv:2203.08828.
- [23] J.-Y. Desaulles, D. Banerjee, A. Hudomal, Z. Papić, A. Sen, and J. C. Halimeh, Weak ergodicity breaking in the schwinger model, *Physical Review B* **107**, L201105 (2023).
- [24] K. Pakrouski, P. N. Pallegar, F. K. Popov, and I. R. Klebanov, Many-body scars as a group invariant sector of hilbert space, *Physical review letters* **125**, 230602 (2020).
- [25] K. Pakrouski, P. N. Pallegar, F. K. Popov, and I. R. Klebanov, Group theoretic approach to many-body scar states in fermionic lattice models, *Physical Review Research* **3**, 043156 (2021).
- [26] P. Kolb and K. Pakrouski, Stability of the many-body scars in fermionic spin-1/2 models, *PRX Quantum* **4**, 040348 (2023).
- [27] F. M. Surace, P. P. Mazza, G. Giudici, A. Lerose, A. Gambassi, and M. Dalmonte, Lattice gauge theories and string dynamics in rydberg atom quantum simulators, *Physical Review X* **10**, 021041 (2020).
- [28] N. Maskara, A. A. Michailidis, W. W. Ho, D. Bluvstein, S. Choi, M. D. Lukin, and M. Serbyn, Discrete time-crystalline order enabled by quantum many-body scars: Entanglement steering via periodic driving, *Phys. Rev. Lett.* **127**, 090602 (2021).
- [29] J.-Y. Desaulles, A. Hudomal, D. Banerjee, A. Sen, Z. Papić, and J. C. Halimeh, Prominent quantum many-body scars in a truncated schwinger model, *Physical Review B* **107**, 205112 (2023).
- [30] D. Banerjee and A. Sen, Quantum scars from zero modes in an abelian lattice gauge theory on ladders, *Physical Review Letters* **126**, 220601 (2021).
- [31] S. Biswas, D. Banerjee, and A. Sen, Scars from protected zero modes and beyond in $u(1)$ quantum link and quantum dimer models, *SciPost Physics* **12**, 148 (2022).
- [32] I. Sau, P. Stornati, D. Banerjee, and A. Sen, Sublattice scars and beyond in two-dimensional $u(1)$ quantum link lattice gauge theories, arXiv preprint arXiv:2311.06773 (2023).
- [33] T. Hayata and Y. Hidaka, String-net formulation of hamiltonian lattice yang-mills theories and quantum many-body scars in a nonabelian gauge theory, arXiv preprint arXiv:2305.05950 (2023).
- [34] D. Banerjee, P. Widmer, F.-J. Jiang, and U.-J. Wiese, Crystalline confinement, arXiv preprint arXiv:1311.2459 (2013).
- [35] D. Banerjee, F. Jiang, P. Widmer, and U.-J. Wiese, The $(2+1)$ -d $u(1)$ quantum link model masquerading as deconfined criticality, *Journal of Statistical Mechanics: Theory and Experiment* **2013**, P12010 (2013).
- [36] D. Banerjee, F.-J. Jiang, T. Olesen, P. Orland, and U.-J. Wiese, From the $su(2)$ quantum link model on the honeycomb lattice to the quantum dimer model on the

- kagome lattice: Phase transition and fractionalized flux strings, *Physical Review B* **97**, 205108 (2018).
- [37] D. Banerjee, S. Caspar, F.-J. Jiang, J.-H. Peng, and U.-J. Wiese, Nematic confined phases in the $u(1)$ quantum link model on a triangular lattice: Near-term quantum computations of string dynamics on a chip, *Physical Review Research* **4**, 023176 (2022).
- [38] M. Troyer and U.-J. Wiese, Computational complexity and fundamental limitations to fermionic quantum monte carlo simulations, *Physical review letters* **94**, 170201 (2005).
- [39] A. Alexandru, G. Başar, P. F. Bedaque, and N. C. Warrington, Complex paths around the sign problem, *Reviews of Modern Physics* **94**, 015006 (2022).
- [40] U.-J. Wiese, Ultracold quantum gases and lattice systems: quantum simulation of lattice gauge theories, *Annalen der Physik* **525**, 777 (2013).
- [41] M. Dalmonte and S. Montangero, Lattice gauge theory simulations in the quantum information era, *Contemporary Physics* **57**, 388 (2016).
- [42] M. C. Banuls, R. Blatt, J. Catani, A. Celi, J. I. Cirac, M. Dalmonte, L. Fallani, K. Jansen, M. Lewenstein, S. Montangero, *et al.*, Simulating lattice gauge theories within quantum technologies, *The European physical journal D* **74**, 1 (2020).
- [43] E. Zohar, Quantum simulation of lattice gauge theories in more than one space dimension—requirements, challenges and methods, *Philosophical Transactions of the Royal Society A* **380**, 20210069 (2022).
- [44] J. C. Halimeh and P. Hauke, Stabilizing gauge theories in quantum simulators: a brief review, *arXiv preprint arXiv:2204.13709* (2022).
- [45] A. Di Meglio, K. Jansen, I. Tavernelli, C. Alexandrou, S. Arunachalam, C. W. Bauer, K. Borrás, S. Carrazza, A. Crippa, V. Croft, *et al.*, Quantum computing for high-energy physics: State of the art and challenges. summary of the qc4hep working group, *arXiv preprint arXiv:2307.03236* (2023).
- [46] R. Brower, S. Chandrasekharan, and U.-J. Wiese, Qcd as a quantum link model, *Physical Review D* **60**, 094502 (1999).
- [47] R. Brower, S. Chandrasekharan, S. Riederer, and U.-J. Wiese, D-theory: field quantization by dimensional reduction of discrete variables, *Nuclear physics B* **693**, 149 (2004).
- [48] S. Chandrasekharan and U.-J. Wiese, Quantum link models: A discrete approach to gauge theories, *Nuclear Physics B* **492**, 455 (1997).
- [49] T. Bhattacharya, A. J. Buser, S. Chandrasekharan, R. Gupta, and H. Singh, Qubit regularization of asymptotic freedom, *Phys. Rev. Lett.* **126**, 172001 (2021), [arXiv:2012.02153 \[hep-lat\]](https://arxiv.org/abs/2012.02153).
- [50] T. V. Zache, M. Van Damme, J. C. Halimeh, P. Hauke, and D. Banerjee, Toward the continuum limit of a $(1+1)$ d quantum link schwinger model, *Physical Review D* **106**, L091502 (2022).
- [51] U.-J. Wiese, From quantum link models to d-theory: a resource efficient framework for the quantum simulation and computation of gauge theories, *Philosophical Transactions of the Royal Society A* **380**, 20210068 (2022).
- [52] J. C. Halimeh, M. Van Damme, T. V. Zache, D. Banerjee, and P. Hauke, Achieving the quantum field theory limit in far-from-equilibrium quantum link models, *Quantum* **6**, 878 (2022).
- [53] See supplementary material at.
- [54] D. Horn, Finite matrix models with continuous local gauge invariance, *Physics Letters B* **100**, 149 (1981).
- [55] P. Orland and D. Rohrlich, Lattice gauge magnets: Local isospin from spin, *Nuclear Physics B* **338**, 647 (1990).
- [56] M. Schechter and T. Iadecola, Many-body spectral reflection symmetry and protected infinite-temperature degeneracy, *Physical Review B* **98**, 035139 (2018).
- [57] V. Karle, M. Serbyn, and A. A. Michailidis, Area-law entangled eigenstates from nullspaces of local hamiltonians, *Physical Review Letters* **127**, 060602 (2021).
- [58] L. Ebner, A. Schäfer, C. Seidl, B. Müller, and X. Yao, Entanglement entropy of $(2+1)$ -dimensional $su(2)$ lattice gauge theory, *arXiv preprint arXiv:2401.15184* (2024).
- [59] J. Osborne, I. P. McCulloch, and J. C. Halimeh, Quantum many-body scarring in $2+1$ d gauge theories with dynamical matter, *arXiv preprint arXiv:2403.08858* (2024).

Supplementary Material for “Quantum Many-Body Scars in $2 + 1$ Abelian Gauge Theories for Arbitrary Integer Spin”

Thea Budde, Marina Krstić Marinković, and Joao C. Pinto Barros
Institut für Theoretische Physik, ETH Zürich, Wolfgang-Pauli-Str. 27, 8093 Zürich, Switzerland
 (Dated: March 29, 2024)

SYMMETRIES OF THE SYSTEMS

The symmetries of the Hamiltonians considered will depend on the choice of the potential. We will always have

- **Translation Symmetry** along the horizontal axis $E_{ni} \rightarrow E_{n+\hat{1}i}$, $U_{n+\hat{1}i} \rightarrow U_{ni}$. Translation along the vertical axis is not always present due to boundary conditions;
- **Reflection Symmetries** with respect to the two axis \mathcal{I}_x and \mathcal{I}_y . Explicitly, \mathcal{I}_x is given by $E_{(n_1, n_2)1} \rightarrow E_{(n_1, -n_2)1}$, $E_{(n_1, n_2)2} \rightarrow -E_{(n_1, -n_2)2}$, $U_{(n_1, n_2)1} \rightarrow U_{(n_1, -n_2)1}^\dagger$, $U_{(n_1, n_2)2} \rightarrow U_{(n_1, -n_2)2}^\dagger$ and analogous for \mathcal{I}_y . These symmetries are important to prove the existence of an exponential number of zero-modes;
- **Charge Conjugation**, which is characterized by the field transformations $E_{ni} \rightarrow -E_{ni}$ and $U_{ni} \rightarrow U_{ni}^\dagger$.

When explicitly referenced, we restricted our exact diagonalization to the zero momentum sector and to the $+1$ charge conjugation sector. Otherwise, the plots are in the electric field basis and no symmetries beyond applying Gauss’ law and being restricted to the zero winding sector are used.

SHANNON AND ENTANGLEMENT ENTROPY

We calculate the Shannon entropy with respect to the electric field basis $\{|\phi_i\rangle\}$. For a state $|\psi\rangle = \sum_i c_i |\phi_i\rangle$, the Shannon entropy has the value

$$S = - \sum_i |c_i|^2 \log |c_i|^2. \quad (1)$$

We split the system into two subsystems A and B of equal size. The bipartite entanglement entropy is then given by

$$S_{\frac{L}{2}} = -\text{Tr} \rho_A \log \rho_A = -\text{Tr} \rho_B \log \rho_B \quad (2)$$

Explicitly, we always partition the system by dividing it vertically into two halves and considering the bordering

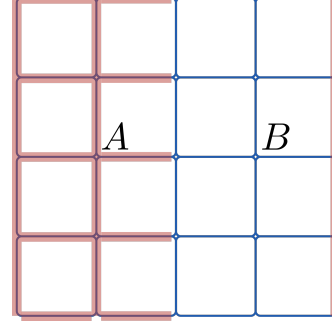


FIG. 1: Example of the partitioning used to compute the entanglement entropy, where the lattice is periodic in the horizontal direction. Both partitions A and B have the same number of links.

vertical links on the left as belonging to the subsystem and the ones on the right as belonging to the other. This is exemplified in Fig. 1.

Low Shannon entropy does not imply low entanglement entropy and vice versa. Still, all the scars we have constructed analytically exhibit both low Shannon entropy and low entanglement entropy. Either measure is therefore able to demonstrate their existence.

INDEX THEOREM AND AN EXPONENTIAL NUMBER OF ZERO-MODES

In [?] it was shown that non-integrable models can still exhibit an exponential number of eigenstates with zero energy. We review this result and adapt it to our models of interest. For this section, we will refer to plaquette flipping terms as the kinetic part of the Hamiltonian

$$K = \sum_n \left(U_{n1}^\dagger U_{n+\hat{1}2}^\dagger U_{n2} U_{n+\hat{2}1} + \text{h.c.} \right). \quad (3)$$

We only need to assume that U_{ni}/U_{ni}^\dagger are operators that raise/lower the value of the electric field on the link by 1. This makes the result very robust with respect to a wide range of formulations.

We define a set of link operators ζ_{ni} , which are diagonal in the electric field basis. For each link we have

$$\zeta|\varepsilon\rangle = (-1)^\varepsilon |\varepsilon\rangle. \quad (4)$$

We further construct

$$\mathcal{C} = \prod_{n=0}^{L_1-1} \prod_{a=0}^{L_2/2-1} \zeta_{(n,2a)1}, \quad (5)$$

where we have assumed L_1 to be even. We can see that \mathcal{C} anti-commutes with the kinetic Hamiltonian $\{\mathcal{C}, K\} = 0$. This implies that if $|E\rangle$ is an eigenstate with energy E , then $\mathcal{C}|E\rangle$ has energy $-E$. In the subspace generated by eigenstates with zero energy, we can diagonalize \mathcal{C} and K together.

Let now \mathcal{I}_y be the unitary transformation that reflects along the vertical axes, as defined above. This is a symmetry of the Hamiltonian and also commutes with \mathcal{C} . We can now use the existence of \mathcal{I}_y and \mathcal{C} to show the existence of an exponential number of zero-modes.

First, note that the number of zero-modes N_0 , is bounded from below by $N_0 \geq |\text{tr}(\mathcal{C}\mathcal{I}_y)|$. We can see this by adopting a basis that diagonalizes both K and \mathcal{I}_y . Such eigenstates are always mapped to a different energy eigenstate by \mathcal{C} unless the energy is zero. As a consequence, only zero-modes contribute to the trace. Each eigenstate, on that sector, will contribute with a value in the interval $[-1, 1]$. This shows that the number of zero-modes can never be smaller than $|\text{tr}(\mathcal{C}\mathcal{I}_y)|$.

We can now show that the trace is actually exponential on the volume by considering the electric field basis. These are all eigenstates of \mathcal{C} , but the only ones surviving the trace are the ones that respect a reflection symmetry along the vertical axis. Such states are fixed by determining the state in half of the volume. The number of these states corresponds to the square root of the total number of states in the whole Hilbert space. By restricting ourselves to specific sectors of the Hilbert space, the two halves are not independent. Nonetheless, we still expect the number of zero-modes to remain exponentially large on the volume.

LEVEL SPACING DISTRIBUTION

We demonstrate explicitly the non-integrability of a single-leg ladder $S = 1$ system in open boundary conditions, by calculating the level spacing distribution. We first resolve the symmetries of the system. Translation symmetry is broken due to the open boundaries. A potential $V = \lambda \sum_n h_n$ is applied, which breaks charge conjugation symmetry. Reflection across the horizontal axis, as defined above, is identical to charge conjugation and is therefore also broken by the potential. Reflections across the vertical axis need to be diagonalized. This results in

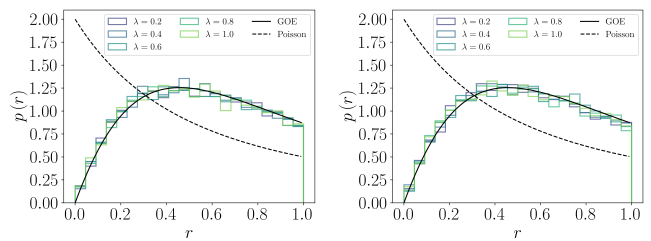


FIG. 2: Level spacing distribution for a single-leg ladder with 12 plaquettes with the height potential at varying λ . With this potential and open boundaries, the model has only reflection symmetry with respect to the vertical axis. This gives rise to two sectors that can be labeled with \pm eigenvalue, whose level distribution is depicted on left and right panels respectively. They match the GOE distribution well, indicating that this system is not integrable.

two sectors, labeled with the eigenvalue ± 1 . The distribution $p(r)$ of consecutive level spacing ratios

$$r_n = \min \left\{ \frac{E_{n+1} - E_n}{E_n - E_{n-1}}, \frac{E_n - E_{n-1}}{E_{n+1} - E_n} \right\} \quad (6)$$

of both sectors match the Gaussian Orthogonal Ensemble (GOE)

$$p_{GOE}(r) = \frac{27}{4} \frac{r + r^2}{(1 + r + r^2)^5/2} \quad (7)$$

as seen in Fig. 2. In contrast, a Poisson distribution

$$p_P(r) = \frac{2}{(1 + r)^2} \quad (8)$$

would be expected for an integrable model.

LOW ENTROPY ZERO-MODES IN TRUNCATED LINK MODELS

Here we describe a generic mechanism to obtain low-entropy mid-spectrum states in the TLM, from the vast space of zero-modes. We start by searching for zero-modes $|\psi_z\rangle$, with a generic decomposition following $|\psi_z\rangle = \sum_n c_i |\phi_i\rangle$, where $\{|\phi_i\rangle\}$ is the electric field basis. By definition, a zero-mode follows

$$K|\psi_z\rangle = \sum_{i,n,\sigma} c_i H_n^\sigma |\phi_i\rangle = 0, \quad (9)$$

where $\sigma \in \{+, -\}$. This is very general and must be satisfied by *all* zero-modes.

Spin- S TLMs have an especially simple structure, which we can use to find low-entropy zero-modes. If $H_n^\sigma |\phi_i\rangle \neq 0$ then $\|H_n^\sigma |\phi_i\rangle\| = 1$ for all n, i and σ . This suggests that we can look for solutions where each term in (9) is canceled by exactly one other term in the sum. In other words, for each non-null term $c_i H_n^\sigma |\phi_i\rangle$,

there exists a term $c_k H_{n'}^{\sigma'} |\phi_k\rangle$ with $c_k = -c_i$ such that $H_n^\sigma |\phi_n\rangle = H_{n'}^{\sigma'} |\phi_k\rangle$ for some σ', n' . This introduces the minimal possible number of non-zero weights to cancel a given $H_n^\sigma |\phi_i\rangle$. In TLMs, states $|\phi_i\rangle, |\phi_k\rangle$ that obey $H_n^\sigma |\phi_i\rangle = H_{n'}^{\sigma'} |\phi_k\rangle \neq 0$, are related by $|\phi_k\rangle = H_{n'}^{-\sigma'} H_n^\sigma |\phi_i\rangle = H_n^\sigma H_{n'}^{-\sigma'} |\phi_i\rangle$.

We then focus on two options to cancel a term $c_i H_n^\sigma |\phi_i\rangle$ in Eq. (9) for TLMs:

1. $|\phi_i\rangle$ is already annihilated by H_n^σ ;
2. The zero-mode also includes the term $-c_i |\phi_k\rangle = -c_i H_{n'}^{-\sigma'} H_n^\sigma |\phi_i\rangle$ with some σ', n' .

The second option not only assures that $H_n^\sigma |\phi_i\rangle - H_{n'}^{\sigma'} |\phi_k\rangle = 0$, but also that $H_{n'}^{-\sigma'} |\phi_i\rangle - H_n^{-\sigma} |\phi_k\rangle = 0$. This means that the contributions $c_i H_{n'}^{-\sigma'} |\phi_i\rangle$ and $c_k H_n^{-\sigma} |\phi_k\rangle$ also cancel each other. What remains are the terms $c_i H_n^{-\sigma} |\phi_i\rangle, c_i H_{n'}^{\sigma'} |\phi_i\rangle, c_k H_{n'}^{-\sigma'} |\phi_k\rangle$ and $c_k H_n^\sigma |\phi_k\rangle$ as well as all terms that act on different sites. These also need to be canceled to get a zero-mode. If it is possible to find a set of states that manage to cancel all contributions in this fashion, this state is a good candidate to be a zero-mode with anomalously low entropy.

Canceling the remaining contributions, could, in principle, be achieved by considering any of these states and acting upon them with another kinetic operator. For example, $H_n^\sigma |\phi_k\rangle$ could be cancelled by adding a state of the form $H_{n''}^{\sigma''} H_n^\sigma |\phi_k\rangle$, for arbitrary choices of n'' and σ'' that do not annihilate the state. To arrive at the zero-modes in arbitrary integer spin, as described in the main text, we choose to cancel them using the same operators as before, so with the state $|\phi_l\rangle = H_{n'}^{-\sigma'} H_n^\sigma |\phi_k\rangle$. This cancels two contributions at the same time, $H_n^\sigma |\phi_k\rangle$ and $H_{n'}^{-\sigma'} |\phi_k\rangle$, further reducing the number of states that need to be included. We then build chains of such states, where both ends are annihilated by the remaining kinetic operators. This way, we build the 2×1 zero-mode state that can be tiled according to the product defined in the following section.

All analytically constructed zero-mode scars that have been derived for the $S = 1/2$ QLM [? ?] have this structure and therefore an equal magnitude of weights for all contributing electric field basis states.

The outlined strategy can be used to construct more zero-mode scars in systems that are not accessible through ED. For other formulations, like QLMs, it will still be true that states that cancel each other in (9) differ by two applications of a kinetic operator. This insight was crucial to understanding the low entropy states observed here for TLMs and may prove useful in the analysis of other systems.

THE TILING PRODUCT

There are multiple options for generalizing scars found in small systems to arbitrarily large lattices. The most straightforward approach is to apply tensor products in the electric field basis. This is only possible if the links at the boundary agree and the resulting system still follows Gauss' law. We generalize this to the *tiling product* \odot , which acts like a tensor product on the dual representation instead. It is defined as

$$|M\rangle \odot |M'\rangle = |MM'\rangle, \quad (10)$$

i.e. the matrices of height variables are concatenated. This is not the tensor product, since the values of the boundary links are added. If the concatenation of M and M' would give rise to an invalid gauge field configuration, i.e. some neighboring height variables satisfy $|h_i - h_j| > S$, we will say that $|M\rangle$ and $|M'\rangle$ *do not tile* and define their tiling product to give the null state. More generally, we are interested in tiling products of the form $(\sum_a c_a |M_a\rangle) \odot (\sum_b c_b |M'_b\rangle)$. We set this product to result in the null state if *any* state in the left-hand side does not tile with *any* state in the right side, otherwise, we just apply the distributive law. In other words, the tiling is distributive if *all* the states in one entry tile with *all* the states in the other.

For example, states that only contain height variables h_i with $\max_i(h_i) - \min_i(h_i) \leq S$, will always tile with themselves. If the difference is larger, one might need to be careful which plaquettes can touch, to prevent neighboring height variables from differing by more than S .

This tiling product gives non-null states (specifically the scars) for the tiles constructed in the main text since $\max_i(h_i) - \min_i(h_i) = S$. In general, scars do not need to have a tiling structure. One eigenstate of E^2 is not composed of tilings. It is described in the following section.

MORE SCARS IN THE PRESENCE OF AN E^2 POTENTIAL

We briefly describe the two other scars present in the 4×4 plaquette system with the potential $g \sum_n E_n^2$. The first one does not have a tiling structure, but a sublattice structure instead. We divide the lattice into two sublattices A and B .

$$|\psi_s\rangle = \frac{1}{2^{L_1 L_2 / 2}} \prod_{m \in A} \left(1 - (H_m^+)^2 P_m^+ - (H_m^-)^2 P_m^- \right) \prod_{n \in B} (H_n^+ - H_n^-) |\mathbf{0}\rangle, \quad (11)$$

where P_m^\pm is the projector on ± 1 on all plaquettes surrounding the plaquette at m . A representation of this state is given in Fig. 3.

0 <i>A</i>	1 <i>B</i>	0 <i>A</i>	-1 <i>B</i>
-1 <i>B</i>	0 <i>A</i>	1 <i>B</i>	0 <i>A</i>
0 <i>A</i>	1 <i>B</i>	2 <i>A</i>	1 <i>B</i>
-1 <i>B</i>	0 <i>A</i>	1 <i>B</i>	0 <i>A</i>

FIG. 3: Representation of a state contributing to a scar for $S = 1$ and E^2 potential that exhibits a sublattice structure. Singlet states are placed in sublattice B while sublattice A is filled by 0's. If all plaquettes surrounding a 0 have the same value of ± 1 , then that plaquette is combined with ± 2 .

T_1	T_8	T_1	T_2
T_4	T_5	T_6	T_5
T_7	T_8	T_7	T_2
T_4	T_3	T_6	T_3

FIG. 4: Schematic representation of a tiling that produces a scar for the E^2 potential in a 4×4 lattice.

This zero-mode is an eigenstate of the E^2 potential because the difference between neighboring plaquettes is always ± 1 , giving all links values with $E_n^2 = 1$. This structure generalizes for arbitrary even L_1 and L_2 .

The remaining observed scar seems exclusive of the 4×4 system. While the fundamental tiling structure still applies, it comes from a different tiling of the states described in the main text. The two plaquettes in a tile lie in the same row or column but have a distance of 2. Explicitly

$$|\psi_s\rangle = \frac{1}{16} \prod_{(n,n') \in T} (H_n^+ - H_{n'}^+) |\mathbf{0}\rangle, \quad (12)$$

where the set of tiles $T = \{T_1, \dots, T_8\}$ is presented in Fig. 4. This tiling guarantees that each T_i shares the same number of neighboring height variables of value 0 and 1 and therefore will be an eigenstate of the potential with eigenvalue $16g$.

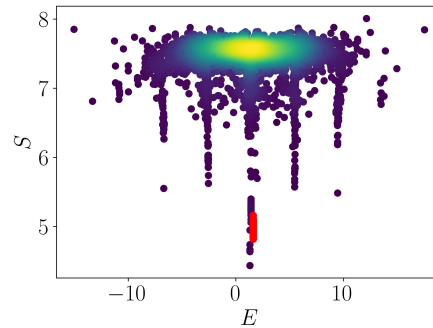


FIG. 5: Shannon entropy of 4×4 $S = 1$ plaquettes with periodic boundary conditions using the Hamming distance potential with a prefactor $\lambda = 0.2$ in the zero momentum and $+1$ charge conjugation sectors. Many mid-spectrum states with low entropy, i.e. scars, are visible. The tower colored in red at $E = 1.6$ contains the predicted scars.

SCARS WITH PERIODIC BOUNDARY CONDITIONS

The scars we have constructed all exist in periodic boundary conditions. A potential that isolates the tower of scars created by the mechanism described in the main text is constructed here. Using the sum of the height variables as the potential is not well defined, since in periodic boundary conditions adding a global constant to all height variables leaves the physical state invariant. Instead, we use the minimum number of kinetic operators that must be applied to the state $|\mathbf{0}\rangle$ to arrive at any given basis state $|\phi_i\rangle$. This is similar to the Hamming distance as used in e.g. [?] generalized for higher spin. The entropy using this potential is shown in Fig. 5, where the tower of predicted scars is visible. Additional towers are present at non-integer multiples of λ , which are not characterized here.

AMPLITUDES OF SCARS

The amplitudes of the isolated low-entropy states match the predictions of the constructed scars. We demonstrate this in the case of the negative energy scars in $S = 1$ single-leg ladders.

The predicted scars with negative energy are generated by tilings of $|\psi_-\rangle$. In the single-leg ladder, only two tilings exist. The two states $|\psi_1\rangle, |\psi_2\rangle$ that these tilings generate are linearly independent and will be in some superposition $|\psi_S\rangle = a|\psi_1\rangle + b|\psi_2\rangle$. All non-zero amplitudes $\langle \phi_i | \psi_{1,2} \rangle$ of both scars are $\pm \frac{1}{\sqrt{2L/2}}$. There are therefore four different possible magnitudes of the amplitudes $A = \langle \phi_i | \psi_S \rangle$:

1. The basis state $|\phi_i\rangle$ has zero overlap with both $|\psi_1\rangle$ and $|\psi_2\rangle$ and therefore the amplitude is zero.

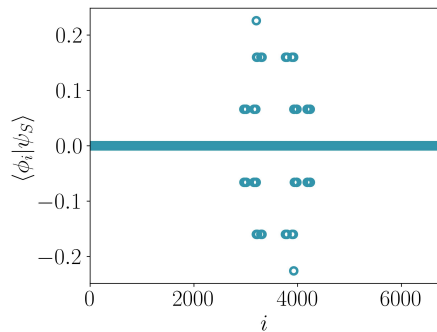


FIG. 6: Overlap of electric field basis states $|\phi_i\rangle$ with the lowest entropy scar in Fig. 3 of the main text. It depicts the entanglement entropy of 10×1 $S = 1$ plaquettes with periodic boundary conditions in the x direction. Most states have zero overlap.

2. The basis state has non-zero overlap with only $|\psi_1\rangle$ and has the amplitude $A = \pm \frac{a}{\sqrt{2L/2}}$.
3. The basis state has non-zero overlap with only $|\psi_2\rangle$ and has the amplitude $A = \pm \frac{b}{\sqrt{2L/2}}$.
4. The basis state has non-zero overlap with both $|\psi_1\rangle$ and $|\psi_2\rangle$ and has the amplitude $A = \pm \frac{a+b}{\sqrt{2L/2}}$.

The fourth case only occurs for the states $|10101010\dots\rangle$ and $|01010101\dots\rangle$, which exist in both tilings.

These four different magnitudes of amplitudes are visible in Fig. 6, which shows the overlap of electric field basis states $|\phi_i\rangle$ with a scar of 10×1 $S = 1$ plaquettes with periodic boundary conditions in the x direction.